THE MUSCLE SPINDLE AS A FEEDBACK ELEMENT IN MUSCLE CONTROL

Lee T. Andrews
Anthony M. Iannone
Medical College of Ohio
Department of Neurosciences
Toledo, Ohio

Donald J. Ewing
University of Toledo
Toledo, Ohio

ABSTRACT

The muscle spindle, the feedback element in the myotatic (stretch) reflex, is a major contributor to muscular control. Therefore, an accurate description of behavior of the muscle spindle during active contraction of the muscle, as well as during passive stretch, is essential to the understanding of muscle control. With this goal in mind, animal experiments were performed in order to obtain the data necessary to model the muscle spindle. Spectral density functions were used to identify a linear approximation of the two types of nerve endings from the spindle A model reference adaptive control system was used on a hybrid computer to optimize the anatomically defined lumped parameter estimate of the spindle. The derived nonlinear model accurately predicts the behavior of the muscle spindle both during active discharge and during its silent period. This model will be used in future research to determine the mechanism employed to control muscle movement.

INTRODUCTION

This paper is concerned with the derivation of a mathematical model which describes the behavior of the mammalian muscle spindle of the cat over its entire operating range. The muscle spindle is a subsystem of a larger system which is responsible for skeletal muscle control. One control loop within this system is known as the myotatic reflex arc.

Analyzing the myotatic reflex itself can be undertaken only when each of the subsystems and elements of this reflex are well defined. It is the goal of this paper to experimentally and mathematically analyze one of the subsystems of the reflex. The subsystem to be considered is the muscle spindle.

The muscle spindle is studied during active contraction as well as during stretch in order to determine the normal functioning of this essential subsystem in the myotatic reflex. An optimization scheme is utilized on an anatomical representation of the muscle spindle in order to ascertain the importance of its various properties. Because it is important to relate each mathematical term to real components within the biological elements themselves, the analysis of the muscle spindle is based on its anatomy rather than treating it as a "spectral fit" of the experimental data. This study utilizes engineering concepts to analyze and predict the normal functioning of the mammalian muscle spindle. These concepts lend themselves to the analysis of this type of biological system because it can be represented as a basic servo mechanism as Merton (1952) did in his well known presentation.

ANATOMICAL CONSIDERATIONS

The mammalian muscle spindle is a complex sensory organ connected in parallel with skeletal muscle fibers. It detects changes in the length of the muscle as well as in other parameters which are related to length, such as tension and velocity. The spindle is composed of several intrafusal muscle fibers contained within one envelope. The multiple fibers contained within this envelope fall into two distinct categories. Of the two fibers, the larger, called the nuclear bag fiber, reveals two different regions. The polar regions of this nuclear bag fiber consist of striated contractile tissue, while the central region is composed of a noncontractile tissue containing nuclei. The smaller fibers within the envelope are a uniform distribution of nuclei and striated regions. These fibers are called nuclear chain fibers due to their chain-like appearance.

Two types of nerve endings innervate the striated regions of the spindle. These are denoted as the γ_1 and γ_2 motor fibers. This gamma efferent system provides the necessary bias to the muscle spindle. Figure 1 shows the γ_1 and γ_2 motor fibers innervating the different types of intrafusal fibers. The afferent discharge from the muscle spindle is of two distinct types. The first, namely, the Ia afferent discharge, has its endings on both the nuclear bag and nuclear chain fibers. These afferent discharges are connected monosynaptically with alpha motoneurons. The second type of discharge, the type II, has its ending only on the nuclear chain fiber and is connected polysynaptically with the alpha motoneuron.

A more detailed discussion of the anatomy of the muscle spindle is available in the list of references: Matthews [2], Eldred [3], Granit [4] and others. Of particular interest are the proceedings of the first Nobel Symposium.

DATA AQUISITION

In order to model a given system, it must be fully defined by certain information. Knowledge of input-output relationships is required to formulate a mathematical description of the system being studied. Therefore, modeling of the muscle spindle requires the recording of input to the spindle as well as its output pulse train. Input to the muscle spindle consists of any mechanical change in the length of the extrafusal muscle fibers. This change

is transferred to the intrafusal fibers of the muscle spindle because the latter are anatomically placed in parallel with the extrafusal fibers. The output of the muscle spindle system includes the afferent discharge of both type Ia (primary nerve ending) and type II (secondary nerve ending) fibers. The following experimental procedures are utilized to obtain the input-output data necessary for modeling the system.

A simple schematic diagram of the experimental facility explains the arrangement of equipment. In Figure 2 the stimulating electrode and monitoring electrodes are shown on the appropriate nerve bundles. The stimulating electrode is driven by a constant current unit to provide uniform stimulus regardless of changes in resistance between the electrode and nerve bundle. The rate and duration of the stimulus pulses are controlled by a stimulator which drives the constant current unit.

Nerve conduction tests are performed in order to differentiate between type Ia and type II nerve fibers from the muscle spindle. A conduction velocity of less than 70 m/sec is generally a type II ending. Further identification of the nerve fibers is made by observing the dynamic sensitivity of the fiber output. The type Ia fiber shows greater sensitivity to velocity of muscle movement than the type II ending.

EXPERIMENTAL RESULTS

A majority of previous investigators have driven the muscle by means of a mechanical apparatus or external force. Such experiments tend to keep the muscle spindle afferent in the range of continuous discharge by controlling the gamma efferent bias and mechanical load. It is assumed that the only region of interest to the physiological system is that of active discharge. This study differs in that it treats the silent period of operation as well as the period of active spindle discharge. This is accomplished by leaving the normal nerve pathways intact and causing muscle contraction by stimulation of the peripheral nerve. The results of these experiments are discussed in detail in succeeding sections.

Isotonic Loading - Type Ia Ending

Isotonic loading of the medial gastrocnemius-soleus muscle group is accomplished by attachment of a constant tension spring. The measurement apparatus provides a low mass mechanism for measurement of muscle movement. After attachment of the spring, the muscle's length is allowed to stabilize. The spindle afferent is monitored in order to ascertain whether the discharge has reached steady state.

Once it has been determined that the muscle spindle and muscle are at steady state, the peripheral nerve to the muscle group is stimulated with a 0.5 millisecond pulse at an amplitude sufficient to cause a maximal twitch of the muscle fibers. This stimulus pulse and the post-stimulus spindle afferent discharge are recorded along with the positional translation of the muscle for a period in excess of one hundred stimuli in order to insure a large enough sample to provide a statistical basis for data analysis.

The resultant positional translation and spindle discharge are shown in Figure 3. It can be seen that the spindle afferent discharge ceases, or is silent, immediately following the stimulus to the muscle. This silent period is maintained until the direction of the velocity component is reversed. Figure 3 also shows that the offset of the silent period is characterized by an apparent bursting or high frequency discharge of the spindle afferent.

The instantaneous frequency of the spindle afferent discharges provides output information to higher centers in the biological system. Therefore, it is an important variable which must be measured. Since each post-stimulus discharge is unique, a post-stimulus histogram of its instantaneous frequency is necessary (Figure 4). This figure illustrates the silent period, its offset, and the instantaneous frequency of the spindle afferent discharge.

Static Characteristics

Observation of static as well as dynamic results are important in understanding the normal function of the muscle spindle. Two types of loads, inertial and isotonic, are utilized to determine the properties of the spindle. These different types of loads affect only the muscle's dynamic response and consequently, the spindle's dynamic response, while the static characteristics of each experiment remain the same. Therefore, the static characteristics for both types of load can be discussed together.

The elastic properties of the muscle are determined by measuring the amount of elongation of the muscle relative to the amount of load. Figure 5 illustrates the results of this measurement for four cats. The four curves shown are displaced in the vertical axis but have similar shapes and appear as a family of curves. The vertical displacement is a natural result of normal differences between experimental animals. The important characteristics to be noted here are the nonlinear nature of the force-displacement curves and the similarity of the curves to each other. The results illustrated in Figure 5 are similar to those of previous investigators. Experiments of Wilkie, 1956; Ritchie and Wilkie, 1958; Zajac, 1968; and others show an exponential relationship between the length of the elastic element and the force applied. However, the results both of this study and the above works disagree with those of Rosenthal [5] who describes the length-tension relationship as one of a linear nature with or without the myotatic reflex present. The data he presented are apparently a result of the dynamic nature under which they were obtained. The nonlinear properties of the elastic element shown in Figure 5 are the result of measurements taken with the myotatic reflex intact.

The static discharge of the spindle, illustrated in Figure 6, has characteristics very similar to those of the length-tension curves graphed in Figure 5. The points plotted in Figure 6 represent the mean spindle discharge; the normal spindle output varies about a mean frequency. Both graphs appear to be logarithmic in nature due to the characteristics of a sharp initial slope followed by continual reduction of slope as the tension is increased.

Inertial Loading - Dynamic Characteristics

Although the static characreristics for both types of loads are the same, the dynamic characteristics are different. A mass is used to provide a load with inertia which more closely approximates the type usually encountered in the normal state. The muscle response and corresponding spindle afferent are shown in Figure 7. The muscle response to the stimuli shows a definite damped oscillation which results in a secondary silent period in the discharge of the spindle afferent. Figure 8 better illustrates the time sequence and duration of this secondary silent period. A family of post-stimulus histograms is illustrated in Figure 9. Whereas the initial silent period remains approximately constant in duration, the secondary silent period diminishes as the load increases and is extinguished by loads in excess of 3.4 kilos. Observation of the family of displacement curves in Figure 10 shows the secondary oscillation of the positional data decreasing as the load is increased. This measure, namely, the sensitivity to secondary oscillations, provides a valuable index of the sensitivity of the spindle afferent to displacement, velocity, and acceleration. Another important phenomenon is the relative constancy of the initial silent period, particularly since the muscle dynamics are grossly affected by increase in load.

The reduction and cessation of pulse discharge during muscle contraction or length decrement can be explained by interpretation of the physical parameters acting on the spindle. The initial silent period observed in Figure 9 cannot be explained simply as a response to the mechanical forces acting on the spindle. Observation of the large variation in muscle response, illustrated in Figure 10, indicates other factors must be present to account for the uniform duration of the silent period. Mechanical factors definitely contribute to the silent period observed in Figure 9. However, as the load is increased, the duration of the silent period does not decrease. The probable cause of the uniform silent period is inhibition of fusimotor neurones by an antidromic volley in adjacent neural roots (Ellaway, 1971; Holmgren and Merton, 1954). This inhibition of fusimotor neurones is shown to have a duration of approximately 50 milliseconds which coincides with the minimum duration of the silent period found in the experimental data. The inhibition of the fusimotor neurones causes the relaxation of the polar regions of the spindle, resulting in the silent period observed in the experimental data. Jansen and Rudjord [7] also noted the same phenomenon and stated, "The duration of the silent period of motoneuron was not appreciably changed even by large variations in the inital tension."

Isotonic Loading - Type II Ending

The exact role of the type II ending in the reflex system is not completely understood. It is thought, however, that the type II ending provides information to the gamma system which controls the efferent bias to the muscle spindle. The data presented in this section shows that the secondary ending of the muscle spindle has very little dynamic sensitivity. Instead, the secondary ending provides a measure of the static position of the muscle. Due to this characteristic, the bias control theory appears to have some validity. However, it is also known that the type II ending excites flexors and inhibits extensors and, therefore, plays additional roles in the overall control system.

Dynamic Characteristics

The spindle afferent discharge and corresponding positional translation are illustrated in Figure 11. Of interest here is the almost complete lack of the typical high frequency discharge noted in previous data at the offset of the silent period. The burst in the afferent discharge readily apparent in the type Ia afferent is drastically reduced in the type II ending. Its afferent discharge frequency decreases gradually as the muscle returns to steady state. Its range of the discharge from the maximum frequency to the steady state frequency is less than twenty percent, whereas the peak discharge rate for the type Ia ending is four to five times that of the steady state discharge.

Discussion of Experimental Results

The preceding sections presented a view of the data generated by the various experiments utilized in this study. This section describes the results and parameters derived from these experimental investigations and discusses them with reference to the results of previous investigators.

The silent period seen in the data presented in this paper demonstrates the nonlinear nature of the type Ia and type II endings. An important parameter to be determined is the sensitivity of the silent period to physical forces. Comparison of the velocity curve and the discharge occurrence histograms shows a relative offset and onset sensitivity of slightly less than 0.1 centimeters per second for offset and approximately 0.9 centimeters per second for onset. Utilizing this sensitivity parameter to determine the load required to extinguish the secondary silent period, a value of 2.7 kilos is determined from the velocity curve in Figure 8. Since only a finite number of loads is used in these experiments, interpolation is necessary to check on the validity of this value. The histograms displayed in Figure 9 show that the secondary silent period is beginning to be extinguished by afferent discharge for a load of 2.270 kilos and is completely extinguished for 3.4 kilos. This agrees very well with the calculated tension of 2.7 kilos. As Lennerstrand states, assessment of velocity response during length decrement cannot be determined. However, the relative values of onset and offset are important in determination of the type of non-linearity in the spindle system. The relative values of these sensitivity parameters are necessary in the prediction of silent period occurrences and durations.

Holmgren and Merton found that an interjected muscle twitch during steady contraction caused a silent period in the electromyogram of the muscle. Before reflex action was developed, the motoneuron discharge was already arrested. This cessation of motoneuron activity was attributed to antidromic blocking, if the twitch was produced by excitation of motor fibers. Similarly, orthodromic stimulation produced a depression in motoneuron activity. In our experiments it is apparent that the silent period onset is attributable to this blocking phenomenon, since the onset of the silent period does not depend on the dynamics of the muscle system. Verification of this phenomenon is also given in the

experiments utilizing inertial loads by observation of the secondary silent period produced. Clearly the onset of the secondary silent period obeys the muscle system dynamics in that case.

Granit and van der Meulen investigated the duration of the silent period and the cause of the spindle afferent's firing after the cessation of activity. The long pause and short pause responses demonstrated were attributed to the large differences in length of the spindles contained within the muscles studied. The adaptation time of spindle length (approximately 10:1 for largest to smallest) to the dynamics of the muscle is described as the predominate cause of the variability in the spindle silent periods. This long pause, short pause phenomenon is not found in the present research. In contrast, the silent period described here is dominated by the dynamics of the muscle itself, with the exceptions already mentioned.

A relatively constant silent period of motoneuron firing was reported by Jansen and Rudjord during single shocks of maximal intensity to the muscle nerve. Three reflex mechanisms were studied in order to determine the cause of the silent period duration. These were: antidromic inhibition, Golgi tendon inhibition, and the pause in Ia excitatory afferent impulses. It was concluded that, under the experimental conditions utilized, the most important factor determining the concomitant silence of the electromyogram was the pause in Ia afferent activity. This agrees with the results shown in the present study as the constancy of the Ia afferent silent period agrees with the motoneuron silent period. However, this research also defines the overall cause of the Ia afferent and motoneuron efferent silent periods, since the motoneuron efferent is dependent on the Ia afferent.

Determination of the frequency of afferent discharge relative to the velocity of the muscle is found by measuring the peak velocity of the preparation and the corresponding peak in afferent discharge. The data for the isotonic and inertial load experiments reveal a nonlinear relationship between velocity and afferent discharge frequency. The probable cause of the differences between the two curves (other than those normally expected between experiments) is the much larger negative velocity of the muscle at the onset of active muscle contraction. This initial large negative velocity component apparently overdrives the system. The nonlinear curves indicate that the muscle spindle can respond only up to certain limits, after which the gain of the system rapidly decreases. This is probably due to depolarization of the nerve terminals in the spindle. Matthews and Stein also observed this nonlinear response in 1969 during sinusoidal changes in muscle length. Their experiments were accomplished through the use of mechanical oscillation of the muscle. however, and cannot be directly compared to this investigation.

THE MODEL

The previous section briefly presented the results of the experiments and analysis of the experimental data. This section utilizes these results in determination of an appropriate model which describes the behavior of the muscle spindle. The model derived is then tested against the experimental data already presented in order to determine the authenticity of its behavior.

Certain constraints, such as approximation of the analog components to the anatomical form of the biological elements, must be maintained. In addition, the model must be able to perform under the influence of forcing functions representing both stretch and contraction. It is with these constraints in mind that the following models are proposed and developed.

Logically, the input or forcing function to the muscle spindle is the displacement of the muscle in which it is contained. Therefore, the muscle itself must be modeled in order to simulate the input in the biological system. The model of the muscle is then used as the input for the model of the muscle spindle.

Analysis of the spectral density function for the muscle shows that a differential equation of at least second order is necessary to describe the response of the muscle. This is determined from the increase in spectral content prior to the decline of the spectral density function. This behavior denotes a complex pair of roots which implies a second order differential equation. Taking this into consideration, the following equation describes such a system.

$$a\ddot{x} + b\dot{x} + cx = f(t)$$

Using mechanical analysis, it is apparent that the three elements in the differential equation represent mass, elasticity, and viscosity. The mass is the lumped sum of the muscle mass and the load to the muscle. Elasticity is the elastic property of the muscle and its interconnecting fibers, and viscosity refers to the viscous properties of the same elements. A model is formulated from these parameters.

Elastic Elements

A reasonable place to begin the modeling process is with the elastic elements of the system. Since the elastic properties of the muscle exhibit their characteristics statically as well as dynamically, the identification scheme can be either static or dynamic. Since static characteristics are described in the previous section and evaluation of the static properties of the element eliminates other dynamic characteristics of the muscle, static evaluation of the muscle fiber is used. Elasticity is analogous to a spring; therefore, it is a simple matter to model the elastic properties with a spring which has the same characteristic behavior as the experimental data. Observation of the data, however, indicates that a linear spring is insufficient to provide an accurate description of the muscle's elastic properties. Therefore, several nonlinear equations are evaluated as to their goodness of fit to the experimental data. The choice of the function for evaluation is somewhat arbitrary, and perhaps other selections would suffice. However, the functions described appear reasonable when observed in relation to the experimental data.

Linear regression techniques are utilized to determine the optimal values of the parameters. Three functions are tested as possible representative lumped parameter estimates of the elastic properties of the muscle fibers. The three choices are as follows:

STRAIGHT LINE ESTIMATE

$$y = ax + b \quad \text{straight line estimate}$$

$$Q = \sum_{i=1}^{n} [Yi - (axi + b)]^2 \quad \text{the cost function}$$

To minimize Q with respect to a and b, the partial derivatives of Q with respect to a and b are equated to zero.

1) $\frac{\partial Q}{\partial a} = -2\sum_{i=1}^{n} [Yi - (ax_i + b)]X_i = 0$

2) $\frac{\partial Q}{\partial b} = -2\sum_{i=1}^{n} [Yi - (ax_i + b)] = 0$

from these equations are obtained

$$a = \frac{\sum_{i=1}^{n} XiYi - \bar{y}\sum_{i=1}^{n} Xi}{[(\sum_{i=1}^{n} Xi)^2 - \bar{x}\sum_{i=1}^{n} Xi]} \quad \text{optimal parameter estimate}$$

POWER ESTIMATE

$$y = ax^b \quad \text{power estimate}$$

$$\ln y = \ln a + b \ln x$$

$y' = a' + bx'$ by using this transformation the previous estimate can be used to determine the transformed parameters.

EXPONENTIAL ESTIMATE

$$y = ae^{bx}$$

$$\ln y = \ln a + bx$$

$y' = a' + bx$ the same technique is utilized to determine the transformed parameters.

The optimal estimates representing the elastic properties of the muscle and its interconnecting tissues are shown in comparison with experimental data in Figure 12. Observation of the graphs shows that the exponential estimate represents the best fit of the experimental data. The power estimate yields a good fit and can also be used as an estimate of the lumped equivalent of the elastic elements. The straight line estimate does not represent a close enough approximation for use in later work.

The estimates derived here are used later in the modeling of the muscle spindle, since it is assumed that the striated regions of the spindle possess properties similar to those exhibited by the muscle itself. The optimal estimates determined are as follows:

$F =$	$1523.8\,X + 0.27$	straight line estimate
$F =$	$1041.3\,X^2$	power estimate
$F =$	$168.25\,(e^{1.91X} - 1)$	exponential estimate

One term of the differential equation has been determined and results in a non-linear differential equation. The second term to be determined is the viscous element in the differential equation.

Viscous Elements

After determination of the elastic properties of the muscle, the next element to be determined represents the viscous property. Viscosity can be represented mechanically by a dash pot. Since the viscous properties of the muscle can only be exhibited during muscle dynamics, the parameter optimization scheme used must be dynamic in nature.

The method used to analyze the viscous properties of the muscle is the gradient search technique. By implementing the differential equation of the system described earlier on the analog portion of the hybrid computer, a dynamic search can be accomplished. Since the properties of the elastic element have been defined, one term of the differential equation is fixed. The term to be optimized is β in the following equation:

$$\alpha\ddot{x} + \beta\dot{x} + cx^2 = f(t)$$

To accomplish this end, experimental data is compared with the data generated by the mathematical model on the analog computer. By summing the square of the difference between the experimental data and the generated data, the error squared cost function is minimized so that the parameter beta (β) is optimized. The cost function is defined as:

$$J = \sum_{i=1}^{n} (XE_i - XM_i)^2 \quad \text{where XE = experimental data}$$

XM = model data

Since the optimal solution is the point where the cost function (J) equals zero, the best estimate of β occurs when the cost is minimized. The value of the model generated data (XM_i) is the voltage sampled by the analog to digital converter at a sample rate determined by the real time clock and the number of clock counts between samples. The sampling rate is a critical factor. If the sample rate of the digital computer deviates too far below the required rate necessary to accurately reconstruct the sampled waveform, the minimized value of the cost function would never approach zero. Taking these factors into account, the following algorithm is implemented in the digital computer:

$$\beta_{i+1} = \beta_i + \lambda \nabla J_i$$

Using the above algorithm, a single parameter search is performed in order to determine the optimal value of beta (β). The results of the optimal search are illustrated in Figure 13. An observation of the graphs shows that an excellent approximation to the experimental data is determined by the following nonlinear differential equation:

$$m\ddot{x} + \beta\dot{x} + cx^2 = f(t) \qquad \text{where } m = 1.0$$

$$\beta = 0.093$$

$$c = 0.915$$

A closer approximation can be obtained by replacing the elastic term with the exponential estimate previously determined. However, due to considerations of ease of implementation on the analog computer, the power estimate is used. The resultant accuracy of the differential equation in relation to the experimental data justifies the deviation from the more optimal estimate of the elastic element in the system.

Muscle Spindle Model

One of the original constraints of the modeling approach previously stated is adherence to anatomical relationships within the structure of the model. Since some of the elements of the model are already defined, the relationship of these elements is determined by referring to the anatomical representation of the muscle spindle shown in Figure 1.

Properties similar to those of striated fibers are assumed and, therefore, the elastic elements are represented by the same nonlinear spring previously derived. The viscous elements are also assumed to possess similar properties to those derived for the muscle in which the spindle is contained. The non-contractile portions of the spindle have been shown to have elastic constants three times greater than that of the striated regions and, therefore, the coefficients of those parameters reflect this difference.

The force generators represented in the lumped parameter model of the spindle are assumed to behave in a manner similar to that already demonstrated by the muscle containing the spindle. However, since the force generators $f_i(t)$ generally provide a bias to the system, a steady state level is used to simulate the force of the striated regions of the spindle. By modification of the model, this force generation system can interact with the model in a manner similar to the muscle itself.

Secondary Ending

The lumped parameter model of the nuclear chain fiber of the muscle spindle is shown in Figure 14. The behavior, or input-output relationships, should correspond to the results elicited by the experimental data. In order to verify these results a comparison of the experimental and mathematical data is a necessity.

The comparison of experimental results with those obtained from the mathematical model is a better test of the model's validity, since the correlation techniques yield only a linear approximation of the nonlinear behavior of the secondary ending. The instantaneous frequency histograms and comparison of actual and artificial unit potentials provide sufficient basis for verification of the model performance.

Instantaneous frequency histograms of experimental and artificial data are shown in Figure 17. The characteristic behavior of the secondary ending is repeated quite accurately by the model for the range of load utilized in the experiments. The artificial data is much more predictable as the random variable of fluctuating γ efferent is not present in the model. This parameter can be added to the model for future studies.

Figure 15 illustrates the similarity of the unit action potential post stimulus firing patterns for the actual and experimental situation. The deviation of the firing pattern of the action potentials of the model is very small in comparison with that of the experimental data. The reasons for this difference are the same as those discussed earlier. The actual sensitivity of the secondary ending to muscle dynamics and to γ efferent bias is easily adjustable in the model and is one of the features which makes the model useful in studying muscle spindle behavior under a variety of system constraints.

Primary Ending

Figure presents the lumped parameter model of the nuclear bag fiber of the muscle spindle. The following differential equations are derived from the model illustrated in Figure 16.

a) $C_1(X - X_1) = C_1(\dot{X}_1 - \dot{X}_2)^2 + B(\dot{X}_1 - \dot{X}_2)$

b) $C_1(X_1 - X_2)^2 + B_1(\dot{X}_1 - \dot{X}_2) = 3C_1\dot{X}_2^2 + B_1\dot{X}_2$

now solving for X_1 from equation (a) yields

$$B_1\dot{X}_1 = B_1\dot{X}_2 + C_1(X - X_1) - C_1(X_1 - X_2)^2$$

$$\dot{X}_1 = \dot{X}_2 + \frac{C_1}{B_1}(X - X_1) - \frac{C_1}{B_1}(X_1 - X_2)^2$$

equation b yields $\dot{X}_2$

$$2B_1\dot{X}_2 = C_1(X_1 - X_2)^2 + B_1\dot{X}_1 - 3C_1\dot{X}_2^2$$

$$\dot{X}_2 = \frac{C_1}{2B_1}(X_1 - X_2)^2 \bullet \frac{\dot{X}_1}{2} - \frac{3C_1}{2B_1}X_2^2$$

The third term shown represents a unindirectional term in the transfer function in as much as the elements represent no load to the system, but are directly responsible for the derivative term in the transfer function of the type Ia ending.

(c) $$KX_3 = B_1(\dot{X}_2 - \dot{X}_3)$$

$$B_1\dot{X}_3 = B_1\dot{X}_2 - KX_3$$

$$\dot{X}_3 = \dot{X}_2 - \frac{KX_3}{B_1}$$

Instantaneous frequency histograms of the model response and experimental response are shown in Figure 17. As can be seen, the behavior of the model closely follows that of the actual biological system. As in the case of the type II ending, the variability of the post stimulus discharge is markedly reduced due to the elimination of the pseudo random variations in the discharge frequency of the biological system.

The post stimulus occurrence histograms shown in Figure 18 also illustrate the ability of the model to approximate the behavior of the muscle spindle primary ending. The sensitivity of the model to variations in velocity is adjustable and, therefore, allows the model to depict wide ranges of conditions normally found in the physical system. This ability of the model to permit adjustment of parameters allows simulation of a great variety of experimental conditions and restrictions.

The Silent Period

One of the goals of this study is to investigate the silent period and to predift its occurrence and behavior. With this purpose in mind, the following silent periods shown in Figure 19 are predicted by the mathematical model. Comparison of the predicted silent periods in Figure 19 with actual silent periods in Figure 20 illustrates the accuracy of the projected calculations.

The explanation for the behavior of the silent period illustrated in Figure 19 is that, once the spindle activity is extinguished, it will remain in this state until it is forced to resume firing. The cause of the resumption in spindle activity shown in illustration is a positive velocity vector greater than 0.9 centimeters per second. This explains why the duration of the silent period increases rather than decreases with load. Initially, it was thought that the silent period would decrease in duration with load until it extinguished due to a reduction in muscle dynamics. However, because of antidromic stimulation, the spindle is initially caused to be silent, regardless of load. · spindle will remain silent for a considerable time (approximately 200 milliseconds) unless something causes it to resume firing. As load is increased, the positive velocity vector exceeds the threshold level with increasing latency. This shift in the time at which the velocity vector exceeds threshold is the cause of the longer duration of the silent period for increased load.

The secondary silent periods for the inertial load experiments illustrated in Figure 9 do not exhibit the phenomenon of increasing duration described in the previous paragraph. The reason for this deviation in the spindle discharge pattern is that the onset of the secondary silent period is due only to the dynamics of the muscle and is not initiated by antidromic stimulation. The model is able to predict these silent periods as well, since both onset and offset of the spindle activity follow the dynamics of the system.

IMPLICATIONS OF THE MODEL

The mathematical model presented, which was derived from experimental data, possesses several capabilities not incorporated in previously published models. Consideration of the entire range of muscle functioning allows the spindle afferent discharge to be predicted both during stretch and active contraction. Additionally, since the elements comprising the model adhere to the anatomy of the muscle spindle, individual parameter contributions to output of the muscle spindle can be studied. Also, sensitivity of the silent period is evaluated and permits the study of the silent period in relation to control of muscle movement.

Since both the muscle and the muscle spindle have been modeled, the control law which governs muscle activity can now be investigated. We can now study the effects of various parameters, such as gamma efferent bias on reflex activity.

Merton's follow-up length servo hypothesis [1], which has been widely accepted as an explanation of muscle control, does not account for phasic muscle movements. His servomechanism can be an adequate mechanism for postural regulation.

Considering the information described in previous sections and by other investigators, spindle discharge mediated by γ activity is inadequate to control muscle movement. In addition, the delays of the γ route due to the propagation time of neural transmission are obvious. A follow-up servo would require a high gain in order to maintain its steady state length, regardless of load. However, the ease with which limb position is varied by application of load verifies the fact that the servo mechanism which controls reflex activity has low gain.

A concept which is taking the place of the follow-up servo theory of muscle control is that of servo-assistance proposed by Matthews [2]. The servo-assistance scheme suggests a system which initiates movement by co-activation of the α and γ pathways. This provides a type of "power steering" whereby contraction of muscle is assisted by increased spindle discharge. However, acceptance of this more plausible explanation of the mechanism of motor control still leaves many factors obscure.

How does the CNS process these and the other sensory inputs such as the Golgi tendon organ and joint receptors? The overall control mechanism appears to utilize all of these inputs to formulate the control strategem.

Given adequate estimators of all of the peripheral receptors and actuators, investigation of the role of the central nervous system plays in tonic and phasic control of muscle movement can be investigated.

1. Merton, P.A.: "Speculations on the Servo-Control of Movement." The Spinal Cord. 1953. Malcom, J.L.; Gray, J.A.B. ed. Ciba Foundation Symposium. Little, Brown & Co., Boston.

2. Matthews, P.B.C.: Mammalian Muscle Receptors and Their Central Actions. Williams & Williams Co. 1972, Baltimore.

3. Eldred, E.: The Dual Sensory Role of Muscle Spindles. Physical Therapy. 1965, Vol. 45, p. 290-313.

4. Granit, R.: The Basis of Motor Control. Academic Press, 1970, London, New York.

5. Rosenthal, N.P.: "A Linear Systems Analysis of the Myotatic Reflex and Its Component." Ph.D. Dissertation, Univ. of Minnesota, 1969.

6. Ellaway, P.H.: "Recurrent Inhibition of Fusimotor Neurones Exhibiting Background Discharges in the Decerebrate and the Spinal Cat." J. Physiol., 1971, Vol. 216, p. 419-439.

7. Jansen, J.K.S.; Rudjord, T.: "On the Silent Period and Golgi Tendon Organs of the Soleus Muscle of the Cat." Acta Physiol. Scand., 1964, Vol. 62, p. 364-379.

8. Gottlieb, G.; Agarwal, G.; Stark, L.: "Studies in Postural Control Systems, Part III: A Muscle Spindle Model." I.E.E.E. Trans. System Science and Cybernetics, Vol. SSC-6, No. 2, April 1970.

9. McRuer, D.T.; Magdaleno, R.E.; Moore, G.P.: "A Neuromuscular Actuation System Model." I.E.E.E. Trans. Man-Machine Systems, Sept. 1968, Vol. MMS-9, p. 61-71.

10. Zajac, F.E.: "The Mathematical Formulation of the Kinematic Properties of Muscle Derived From an Experimental Investigation." Ph.D. Dissertation, Stanford University, 1968.

11. Houk, J.C.; Cornew, R.W.; Stark, L.: "A Model of Adaptation in Amphibian Spindle Receptors." J. Theoret. Biol., 1966, Vol. 12, p. 196-215.

12. Rudjord, T.: "A Second Order Mechanical Model of Muscle Spindles Primary Endings." Kybernetic, 1970, Vol. 6, p. 205-213.

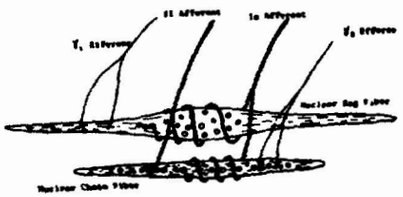

Figure 1

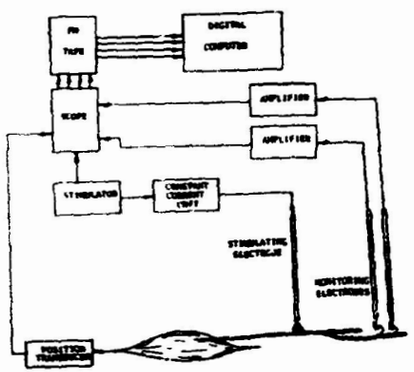

Figure 2

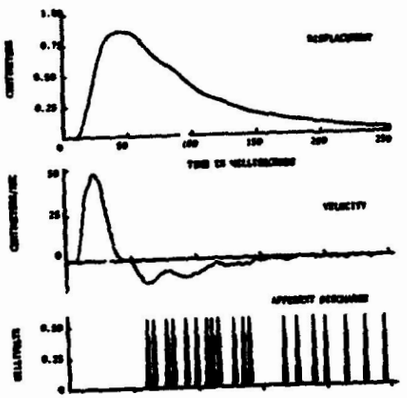

Figure 3

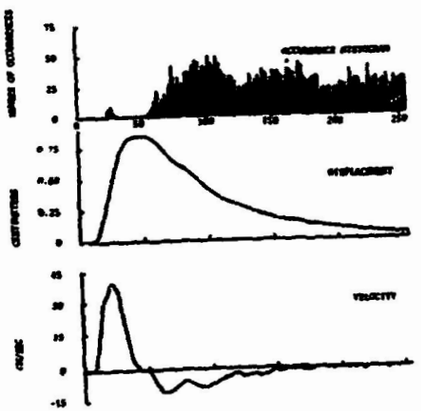

Figure 4

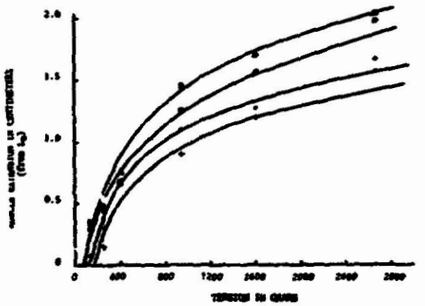

Figure 5

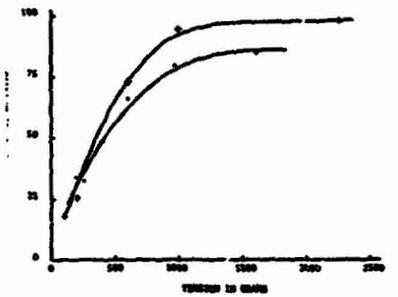

Figure 6

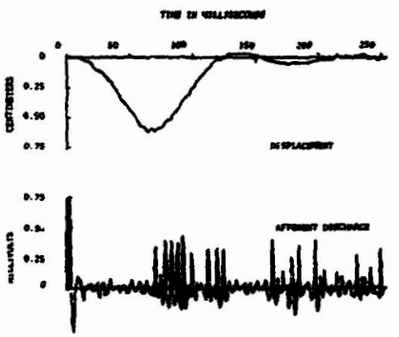

Figure 7

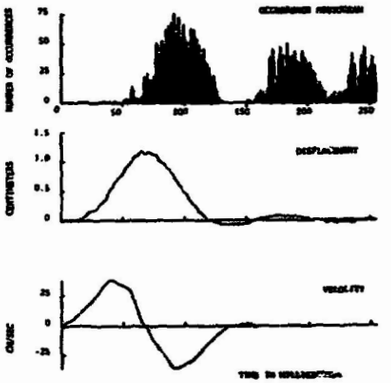

Figure 8

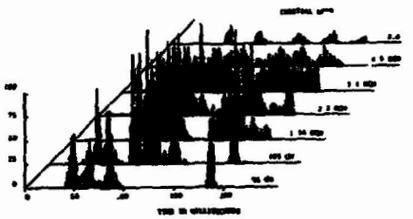

Figure 9

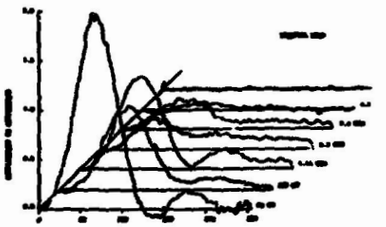

Figure 10

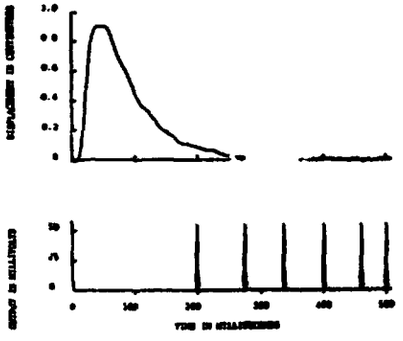

Figure 11

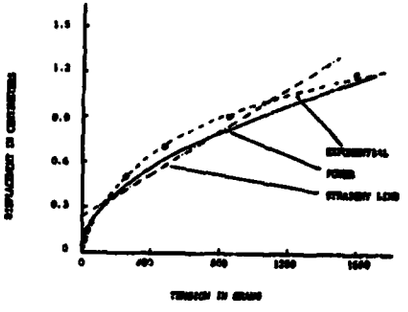

Figure 12

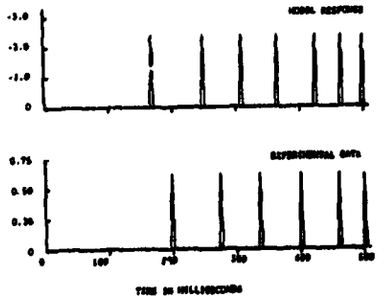

Figure 15

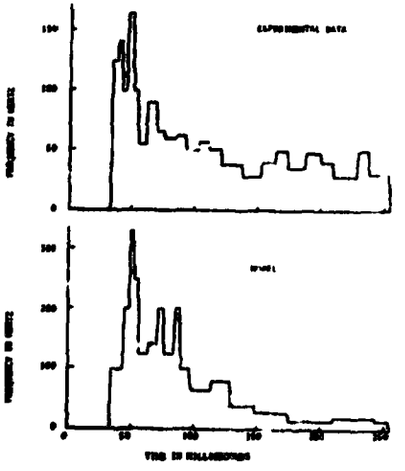

Figure 17

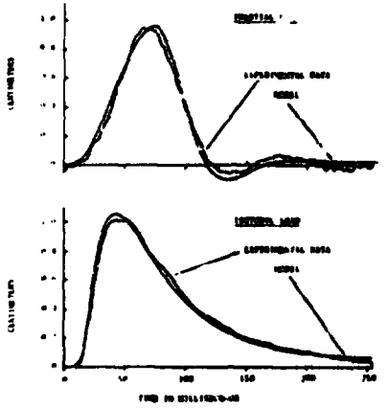

Figure 13

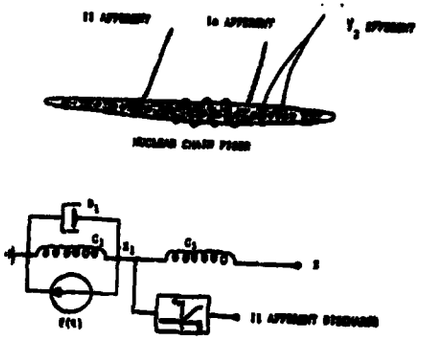

Figure 14

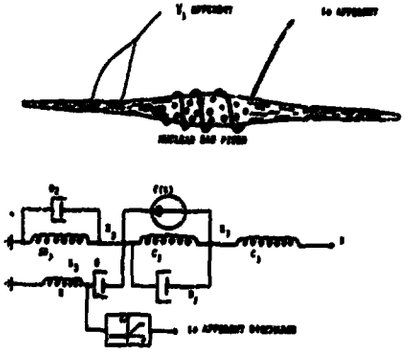

Figure 16

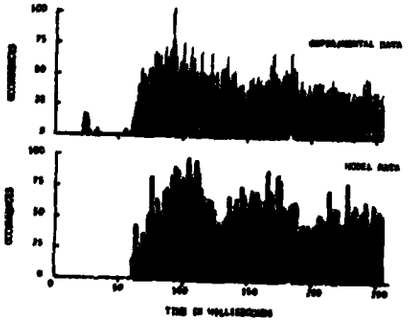

Figure 18

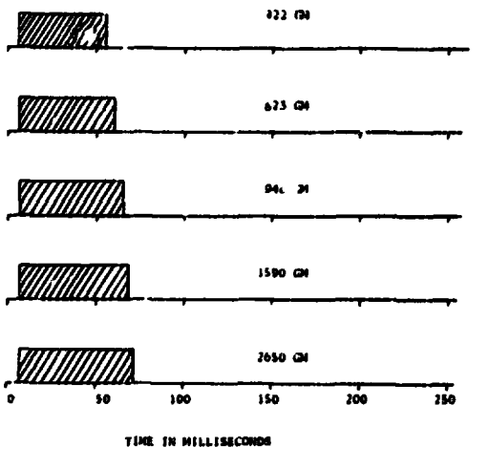

Figure 19

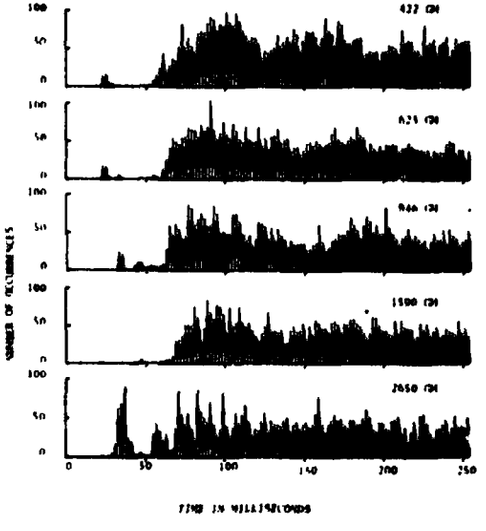

Figure 20